

Article

Effect of Deformation Degree on Microstructure and Properties of Ni-Based Alloy Forgings

Ruifeng Dong ^{1,*} , Jian Li ¹ , Zishuai Chen ², Wei Zhang ¹ and Xing Zhou ¹

¹ College of Materials Science and Engineering, Inner Mongolia University of Technology, Hohhot 010051, China

² College of Materials Science and Chemical Engineering, Harbin University of Science and Technology, Harbin 150040, China

* Correspondence: drfcsp@imut.edu.cn

Abstract: The primary objective of this paper is to investigate the influence of deformation degree on the microstructure and properties of a Ni-based superalloy. An upsetting experiment was conducted using a free-forging hammer to achieve a deformation degree ranging from 60% to 80%. The impact of the forging deformation degree on the hardness and high-temperature erosion performance was evaluated using the Rockwell hardness tester (HRC) and high-temperature erosion tester, respectively. The experimental results indicate that as the deformation degree increased, the hardness of the forged material progressively increased while the rate of high-temperature erosion gradually decreased. In order to comprehensively study the mechanism behind the variations in forging performance, optical microscopy (OM), scanning electron microscopy (SEM), electron backscatter diffraction (EBSD), and transmission electron microscopy (TEM) were employed. The findings reveal that as the deformation degree increased, the presence of small-angle grain boundaries and an increase in grain boundary area contributed to enhanced hardness in the alloy forgings. Furthermore, it was discovered that grain boundaries with twin orientation promoted dynamic recrystallization during deformation, specifically through a discontinuous dynamic recrystallization mechanism. Additionally, the precipitated γ' phase in the alloy exhibited particle sizes ranging from 40 to 100 nm. This particle size range resulted in a higher critical shear stress value and a more pronounced strengthening effect on the alloy.



Citation: Dong, R.; Li, J.; Chen, Z.; Zhang, W.; Zhou, X. Effect of Deformation Degree on Microstructure and Properties of Ni-Based Alloy Forgings. *Metals* **2024**, *14*, 340. <https://doi.org/10.3390/met14030340>

Academic Editors: Andrea Di Schino, Boris B. Straumal and Claudio Testani

Received: 14 August 2023

Revised: 18 September 2023

Accepted: 26 September 2023

Published: 15 March 2024



Copyright: © 2024 by the authors. Licensee MDPI, Basel, Switzerland. This article is an open access article distributed under the terms and conditions of the Creative Commons Attribution (CC BY) license (<https://creativecommons.org/licenses/by/4.0/>).

Keywords: deformation degree; erosion rate; low angle grain boundary; precipitated phase

1. Introduction

Superalloys are alloys that exhibit exceptional resistance to deformation and maintain their functionality under high external forces and temperatures exceeding 600 °C. The performance of fighter aircraft heavily relies on their cutting-edge aeroengines, which predominantly utilize superalloys. Consequently, research and development on superalloys have become globally significant strategic topics. The United Kingdom, the United States, and the former Soviet Union were the initial pioneers in superalloy production. The United Kingdom, as the forefather of superalloys, has established two distinct systems: cast superalloys and wrought superalloys. The primary utilization is focused on nickel-based wrought superalloys. Simultaneously, the United States played a creative role by introducing powder superalloys, incorporating elements such as cobalt, molybdenum, tungsten, and others into nickel-based alloys to produce various grades of superalloys with different service temperature capabilities. Currently, the United States boasts the widest variety and highest quality of superalloys worldwide. Following suit, China embarked on high-temperature alloy research and development [1–4].

In comparison to international efforts, China's research and development in high-temperature alloys started relatively later. The first high-temperature alloy brand was a replica of the Soviet Union's GH3030. Subsequently, several successful high-temperature alloys were developed, including GH3044, GH4033, and GH2036 [5]. Iron-based superalloys

fail to meet the demands of aerospace development due to their lower service temperature. With limited cobalt reserves in the natural environment, the development of cobalt-based superalloys gained prominence. As a result, Chinese researchers shifted their focus to the creation of nickel-based superalloys, with particular attention given to GH4738, a widely utilized nickel-based superalloy [6].

This research investigates the influence of deformation degree on the microstructure and characteristics of nickel-based superalloys, specifically focusing on GH4738 alloy, a phase precipitation hardening type of deformed nickel-based superalloy. Below 760 °C, this alloy exhibits excellent tensile strength and durability, while below 870 °C, it demonstrates outstanding oxidation resistance. Because of its strong crack propagation resistance and corrosion resistance, GH4738 alloy is widely used in turbine disk components of aero engines [7–10]. However, due to the high-volume percentage of the γ' phase (approximately 23.5%), achieving microstructure uniformity during the forging process becomes challenging. The uniform distribution of grains and dispersed γ' phase in forgings is crucial for ensuring superior mechanical properties in wrought superalloys [11,12]. Moreover, GH4738 alloy contains a significant amount of alloy elements, leading to substantial solid solution and precipitation strengthening effects, which further complicates subsequent processing [13]. Thus, reasonable deformation process parameters are essential for achieving a homogeneous microstructure in alloy forgings [14]. Therefore, optimizing the hot deformation process of this alloy holds great importance in controlling grain size, γ' phase size, and distribution after deformation. These optimizations can enhance the alloy's stability, extend its useful life, and improve its overall mechanical properties, considering its high service temperature and creep qualities [15].

Apart from deformation-related investigations, it is also crucial to examine high-temperature erosion wear, which refers to the material loss, fracture, or displacement caused by repetitive impacts of solid particles on a solid surface. Dust ingestion during engine operation accelerates wear and shortens the engine's lifespan. Hence, researching the performance of high-temperature erosion wear is vital for increasing engine longevity [16].

Through quantitative description, Li Wang et al. [17] constructed a thermal processing map to determine the ideal deformation process parameters based on microstructure evolution during thermal deformation. In a systematic investigation of the GH4738 alloy's dynamic recrystallization microstructure distribution under hot processing factors, Liu Hui [18] obtained specific results. Additionally, several studies have been conducted on the rheological mechanical behavior and microstructure evolution of the GH4738 alloy during hot deformation [19–21]. However, all of the aforementioned researchers utilized the Gleeble-1500 thermal simulation testing apparatus, which resulted in a slight disparity between the experimental conditions and actual production. To study the creep behavior of a Ni-based solid solution-reinforced NiMoCr alloy under different hot rolling and cold rolling process conditions, T. Kvackaj et al. [22] discovered that the failure process involves fracture nucleation and crack propagation, both of which are strongly influenced by grain size. It was found that the fine recrystallized structure exhibits significantly lower creep resistance compared to the coarse grain size. Therefore, this study focuses on investigating the hot working process scheme of the GH4738 alloy turbine disk using the free forging process under identical deformation temperatures and varying degrees of deformation. Hot deformation tests were performed on GH4738 alloy bars with different levels of deformation to examine grain refinement behavior and the mechanism of recrystallized grain nucleation post-deformation. Analyzing the alloy's strengthening mechanism after deformation will facilitate the design and optimization of deformation process parameters for GH4738 alloy bars, based on both experimental and theoretical approaches.

2. Experimental Material and Methods

Vacuum consumable remelting (VAR) and vacuum induction melting (VIM) were employed to create the GH4738 alloy that was used in this study. The 200 mm billet was

produced after billet opening and homogenization treatment. The chemical make-up of the nickel-based superalloy GH4738 is shown in Table 1.

Table 1. Chemical composition table of GH4738 superalloy (mass %).

Element	C	Cr	Co	Mo	Al	Ti	Fe	Ni
Mass %	0.035	19.41	13.22	4.30	1.35	2.98	1.00	bal

As shown in Figure 1, four small rod blanks, each with a diameter of 45 mm, were extracted at intervals of 200 mm to ensure consistency in the initial tissue state. The rod billet was then heated in a stepwise manner to a temperature of 1140 °C in the heating furnace. Immediately after heating, the billets were taken out and subjected to repeated upsetting using a 1 t free forging hammer. This process transformed the four rod billets into disk forgings at a height of 80 cm from the material. The undercutting rates employed were $5 \times 10^{-2} \text{ s}^{-1}$, $6 \times 10^{-2} \text{ s}^{-1}$, $7 \times 10^{-2} \text{ s}^{-1}$, and $8 \times 10^{-2} \text{ s}^{-1}$. Subsequently, the forged disk forgings were placed in designated positions for cooling, ensuring that they retained their shape without any deformation. The forged disks exhibited no signs of deformation cracks. The specific details of the thermal deformation process are outlined in Table 2.

Table 2. Actual thermal processing parameters of the samples.

Scheme	Deformation Temperature (°C)	Billet Size (mm)	Finished Size (mm)	Deformation Degree (%)
1	1140	$\phi 45 \times 110$	$\phi 69 \times 42$	62
2			$\phi 76 \times 35$	68
3			$\phi 82 \times 30$	72
4			$\phi 92 \times 23$	80

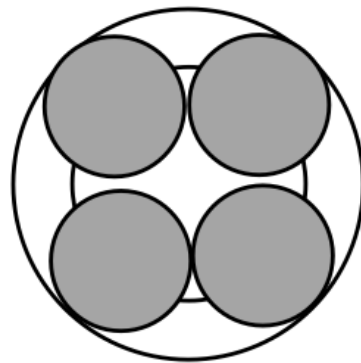


Figure 1. Schematic diagram of the material selection location.

To obtain samples of $10 \times 10 \times 10$ mm dimensions, disc forgings with varying degrees of deformation were cut along the 1/4 diameter direction. Electrolytic polishing, electrolytic corrosion, and polishing were necessary for metallographic observation. Electrolytic removal of surface scratches resulted in a clearer metallographic image. An etching agent of 3 g CuCl_2 + 20 mL HCl + 30 mL $\text{C}_2\text{H}_5\text{OH}$ was used, while the voltage and time for electropolishing, as well as the polishing solution, were both at 20% HCl and 80% CH_3OH . SEM and EBSD were utilized for observations. The electrolytic corrosion solution consisted of 170 mL H_3PO_4 + 10 mL H_2SO_4 + 15 g Cr_2O_3 at a voltage of 3–5 V and time range of 5–10 s. The microstructure of the four groups of samples was examined using Zeiss metallographic and scanning electron microscopes (Oberkochen, Germany) to study the size, size distribution, and size variation of precipitated phases and grains under varying degrees of deformation. The nucleation mechanism of recrystallized grains, substructure changes, and γ' phase evolution during hot deformation of the alloy were studied using EBSD and a transmission electron microscope.

The HR-150A Rockwell hardness tester (Lanzhou Zhongke Kaihua Technology Development Co. China, Lanzhou, China) was utilized to examine the hardness variations of the four sample groups. The process involved testing five samples from each group, eliminating the highest and lowest values, and calculating the average as a representation of the sample's hardness. For the high-temperature erosion wear test, the ASTM G76 high-temperature erosion wear test machine was employed. A 50 mm by 50 mm by 10 mm sample was used for this test. The experimental process entailed the following details: The abrasive temperature was set at 750 °C, with an objective temperature of 750 °C. A total of 2 kg of abrasive was used, and the erosion speed was maintained at 88 m/s. The erosion angle was set to 90°, and the erosion time was 20 s. Under these conditions, the morphology of the GH4738 alloy, subjected to various degrees of distortion due to high-temperature wear, was examined, along with the influence of hardness on high-temperature wear.

To prepare material samples for transmission electron microscopy (TEM) investigation, a square sheet measuring 8 × 8 × 2 mm was thinned using metallographic sandpaper until it reached a thickness of under 65 μm. The electrolyte used for the preparation of these sheet samples in TEM was a mixed solution consisting of 10% HClO₄ and 90% C₂H₅OH. The preparation was carried out in a current environment ranging from −40 °C to −35 °C, with a voltage of 50 V and a current intensity of 40 mA to 45 mA.

3. Results and Discussion

3.1. Effect of Deformation Degree on Microstructure of Ni-Based Alloy

The microstructure of the GH4738 alloy under various degrees of deformation is shown in Figure 2. The figure illustrates how, following the upsetting deformation experiment, the sample's grain size steadily reduced as the degree of distortion increased and there was no mixed crystal. The image also shows that the samples with the four deformation degrees had two sizes of grains, with the smaller grains around the bigger grains. This event shows that recrystallization is essentially finished. At the same time, when the degree of deformation is very low, the deformation is too slight, and the stored energy is insufficient to cause recrystallization; thus, the change in grain size is not immediately apparent. The grains are refined following recrystallization when the deformation exceeds the critical deformation, and the bigger the deformation is, the finer the grains become. Because the nucleation rate grows quickly and the stored energy driving nucleation and growth increases constantly as the deformation size increases, refining occurs as the G/N ratio decreases.

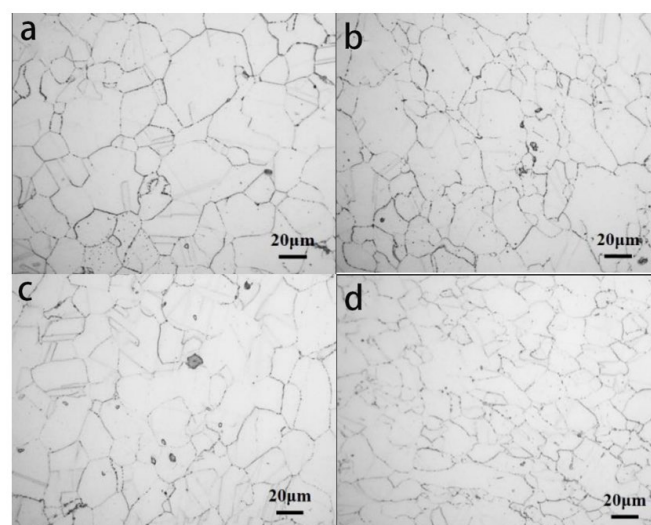


Figure 2. Microstructure of forgings of the GH4738 alloy with different degrees of deformation: (a) 62%; (b) 68%; (c) 72%; (d) 80%.

The precipitated γ' phase diagram of GH4738 alloy forgings at various degrees of deformation is shown in Figure 3. The size of the γ' phase in forgings steadily reduced with the increasing deformation amount, as indicated in the figure, although the amount of γ' phase precipitation did not significantly increase. The grain border area was expanded as the grain size was gradually fine-tuned. During the deformation process, this effect encouraged the diffusion of solute atoms. As a result, the size of the γ' phase in the sample was finer and more uniform, and it had a tendency to be spherical. The foundation for the dispersion distribution of the γ' phase is laid by the uniform distribution of solute atoms in the matrix [23,24].

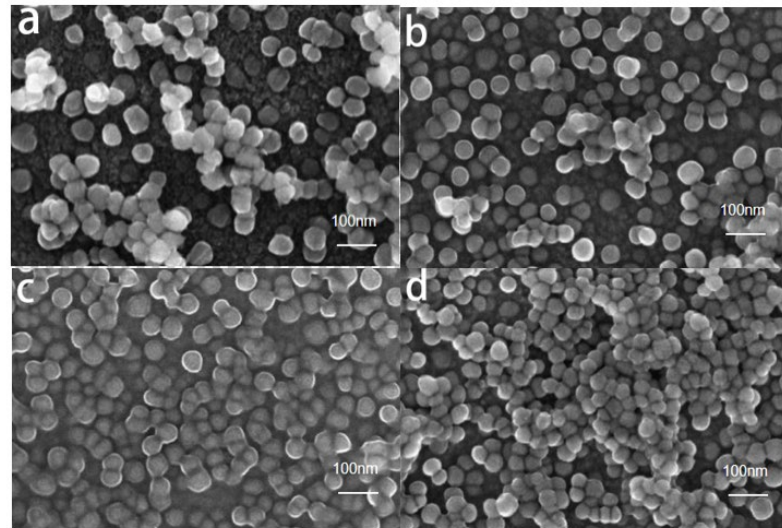


Figure 3. γ' phase in GH4738 alloy forgings at different deformation levels: (a) 62%; (b) 68%; (c) 72%; (d) 80%.

3.2. Effect of Deformation Degree on Properties of Ni-Based Alloy

The average grain size, γ' phase particle size, and hardness of samples with varying degrees of deformation are compared in Figure 4. The Image J software 2.3.0 (National Institutes of Health, Bethesda, MD, USA) was used to measure the diameter of each grain in the optical microscopy (OM) images, enabling the determination of the average grain size. Measurements were taken from three different angles and typical orientations for each grain, and the average value was derived from these three sets of data. The grains in the images were categorized, and the distribution percentage for each grade was determined based on the ASTM grade list and the measured values. Thus, the average value of grains within the same grade was obtained. The average grain size of the material was calculated by summing the average value and the proportion of grains in each grade. The “phase” amount in the image, referred to as “phase size,” was determined using the Image Pro Plus software 6.0 (Media Cybernetics, Rockville, MD, USA) by calculating the percentage of the pixel area occupied by the brightest “phase” in the image. Each test group was counted three times, and the average value was calculated. According to the diagram, significant levels of deformation can result in the formation of fine and uniform grains as well as the γ' phase. Furthermore, it leads to an increase in hardness from 38.9 HRC to 44 HRC. Grain refinement serves to provide a strengthening effect through the presence of fine grains. Additionally, under substantial degrees of deformation, complete recrystallization may occur, resulting in the formation of a strong material [25,26].

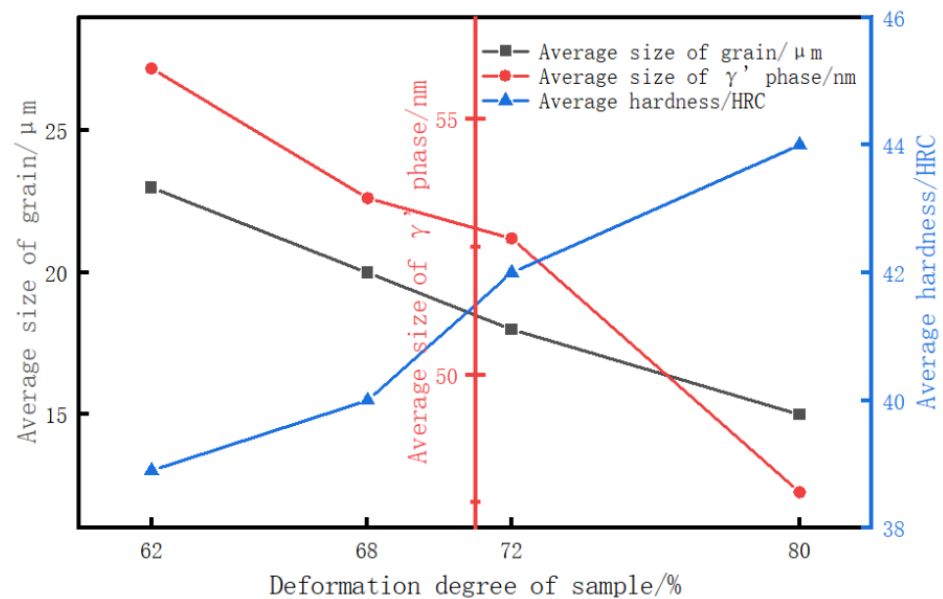


Figure 4. Comparison of average grain size, γ' phase particle size, and hardness of samples with different deformation degrees.

Figure 5 presents the morphology of high-temperature erosion observed using various methods. The image reveals an increased number of craters and a slight cutting effect, indicating the prevalence of impact deformation mechanisms. Figure 6 illustrates the impact of deformation degree on the hardness and high-temperature wear rate of GH4738 alloy. It can be observed that as the degree of deformation increased, so did the hardness. Calculations demonstrate that the hardness at 80% deformation was 14.3% higher than that at 62% deformation. At a deformation degree of 62%, the sample surface exhibited low strength, making it vulnerable to erosion and wear. Consequently, the erosion pits displayed a significant amount of cutting, which limits plastic deformation. Moreover, through computation and comparison, it was determined that the sample with an 80% deformation degree exhibited a reduced high-temperature erosion rate, which decreased by 10.3% compared to the sample with a 62% deformation degree. Furthermore, it is worth noting that the harder the alloy is, the faster it tends to corrode at high temperatures. The mechanism of partial dislocation cutting the small size phase of the GH4738 alloy under various processes undergoes changes during high-temperature erosion at 750 °C. This leads to a decrease in intracrystalline strength to some extent but an increase in plasticity at high temperature. However, the grain boundary strengthening mechanism provides better resistance against high-temperature erosion. When the content of the phase is close to or equal to the grain boundary fraction, grain boundary strengthening becomes the dominant mechanism in enhancing resistance to high-temperature erosion.

3.3. The Nucleation Mechanism of Recrystallized Grains in the Alloy and the Evolution of Substructure Inside the Grains

Researchers can utilize Electron Backscatter Diffraction (EBSD) to investigate the mechanism of dynamic recrystallization in alloys by analyzing orientation, microstrain, and dislocation density. Dislocation density provides insights into the presence of substructures within a specific area and can be determined by comparing the cumulative orientation angle along a designated line. In a study conducted by Azarbarmas et al. [27], the EBSD technique was employed to analyze the dynamic recrystallization behavior of In718 alloy during thermal deformation. By examining the cumulative orientation angle within the deformed grains, it was observed that most subgranular boundaries were still forming at lower strains, indicating the absence of continuous dynamic recrystallization (CDRX). However, as dynamic recrystallization (DRX) progressed under higher strains, strain-

free grains emerged, leading to a gradual decrease in dislocations and a reduction in the occurrence of small-angle grain boundaries. At this stage, medium to high angular dislocation boundaries were observed near the original grain boundaries, signifying the influence of successive progressive subgrain rotations and promoting CDRX at higher strains. Hence, the primary deformation mechanism identified for the In718 alloy at lower strains is the dynamic discontinuous recrystallization (DDRX) mechanism. However, as the strain increases, the prevalence of the CDRX mechanism becomes more pronounced.

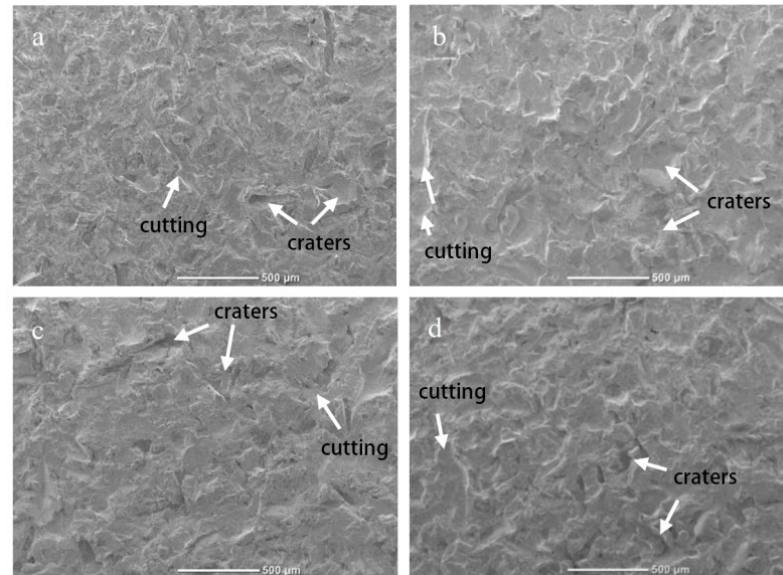


Figure 5. High-temperature erosion morphology of specimens with different degrees of deformation: (a) 62%; (b) 68%; (c) 72%; (d) 80%.

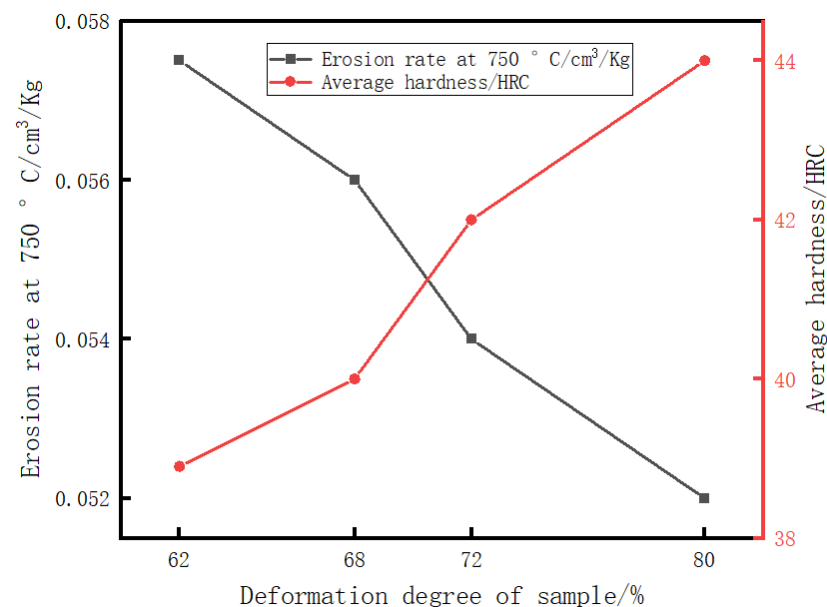


Figure 6. Effect of deformation degree on hardness and high temperature wear rate of the GH4738 alloy, cm³/Kg.

The distribution diagram in Figure 7 shows the grain boundaries of the GH4738 alloy with different phase differences, while the EBSD diagram displays the alloy's microstructure. It can be observed from Figure 7a that the forging had a consistently small grain size. The presence of carbides inhibited the migration of original grain boundaries, leading to a

significant increase in the nucleation rate of recrystallized grains. Recrystallization in this alloy was primarily achieved through dynamic recrystallization (DDRX). Figure 7b reveals that large angle grain boundaries accounted for 43% of the deformation in GH4738 alloy forgings, while small-angle grain boundaries accounted for 56%. There were relatively few medium-angle grain boundaries, and their characteristics were similar. Figure 7c illustrates the distribution of various phase differences (ranging from 0° to $2\text{--}5^\circ$) at low-angle grain boundaries in GH4738 alloy. When the proportion of 2° phase differences in these boundaries reaches around 80%, it indicates the presence of subgrain boundaries and dislocation substructures in the alloy. During the hot processing of highly deformed alloys, a large number of dislocations interact with grain boundaries, resulting in dislocation entanglement and stacking, which contributes to the development of substructures within the alloy [28]. In metals with low stacking fault energy, complete dislocations tend to transform into partial dislocations with lower energy, thereby promoting the formation of twin structures and improving overall performance.

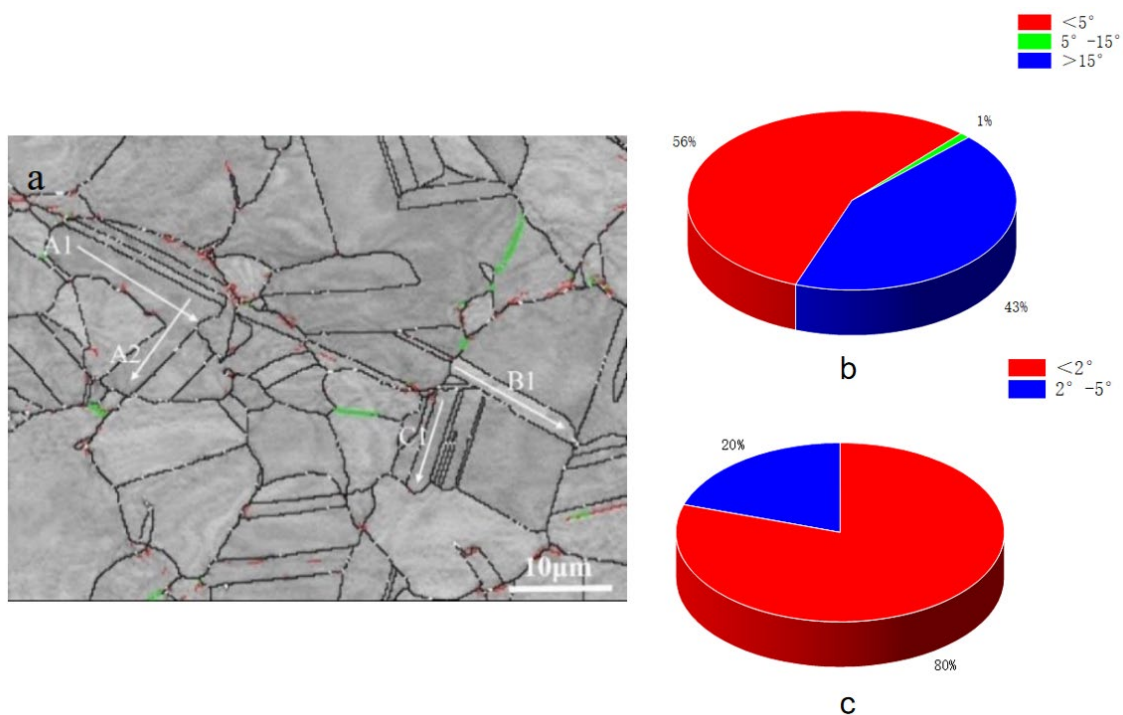


Figure 7. EBSD diagram and distribution pattern of grain boundaries with different phase differences for GH4738 alloy. (a) EBSD diagram of forgings with a deformation of 80%; (b) the distribution of grain boundaries with orientation differences in different states of the alloy; (c) the distribution of $<2^\circ$ and $2\text{--}5^\circ$ orientation difference grain boundaries in different states of the alloy.

The distribution of the orientation angle along Figure 7a along straight lines is illustrated in Figure 8. According to the analysis of cumulative orientation angles in figures, the highest cumulative orientation angle of deformed grains in GH4738 alloy forgings was only 5.8° . During the heating process prior to forging, the second phase in the alloy and the majority of primary carbides have completely returned to the matrix [29,30]. Consequently, there was minimal presence of precipitated phases impeding the grain boundary during deformation. The primary mechanism for the nucleation of recrystallized grains was the initial bending of the grain boundary, while the major nucleation process was the discontinuous dynamic recrystallization mechanism. The granular M23C6 carbides were dispersed and precipitated on the recrystallized grain boundaries and twin boundaries during the cooling process following deformation. This formed the basis for alloy strengthening through the pinning of recrystallized grain boundaries and twin boundaries.

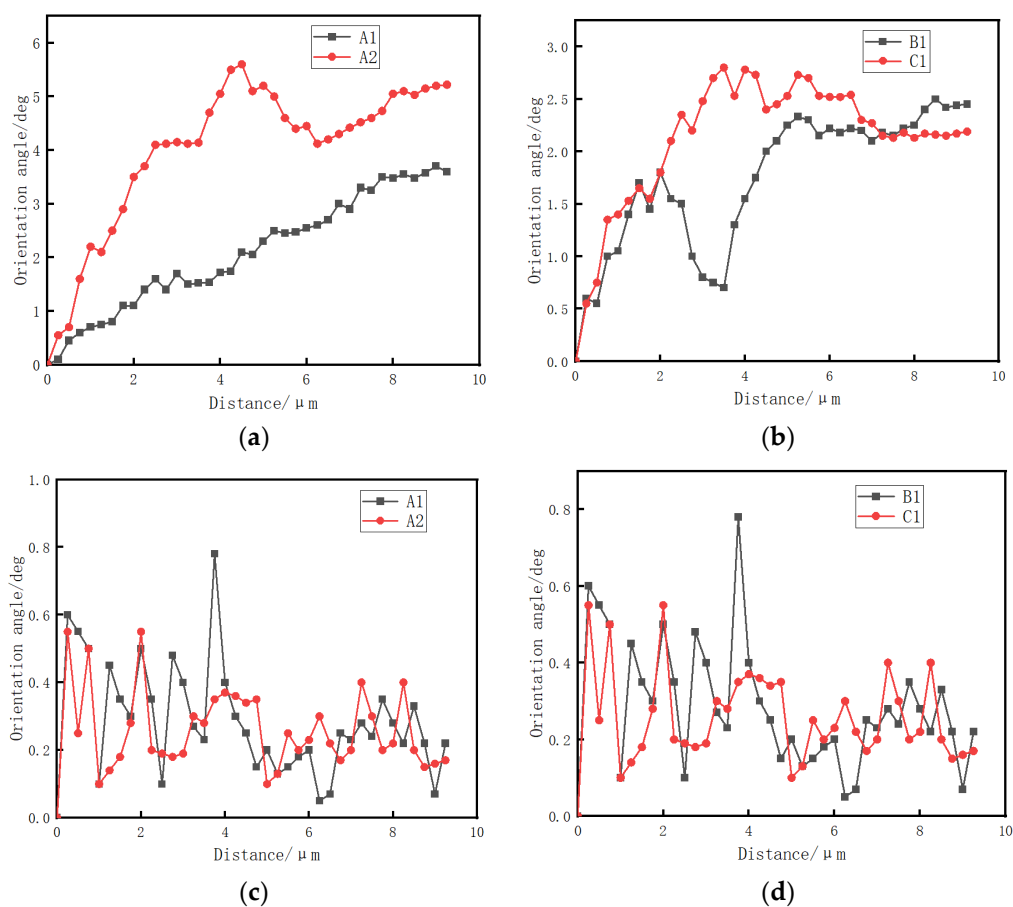


Figure 8. Distribution of orientation angles along the direction of the straight-line segment in Figure 6. ((a,b) Point to origin, (c,d) point to point).

The nickel-based superalloy layer exhibited a low fault energy, which enhanced the likelihood of twin formation during deformation. The dynamic and static recrystallization processes lead to the creation of different types of stepped grain boundaries due to the transition from regular crystal to the low refractive index crystal plane. This transition reduces energy and widens the grain boundary [31]. Twin formation reduces the grain boundary energy of recrystallized grains, thereby promoting dynamic recrystallization. In the heat deformation process of alloy GH4738, primary $\Sigma 3$ twin boundaries with a 60° orientation and $\Sigma 9$ twin boundaries with a 28.9° structure were observed. The “coincidence site lattice” rule [32] states that the interaction of two $\Sigma 3$ twin boundaries can generate a $\Sigma 9$ twin boundary, the interaction of a $\Sigma 3$ and $\Sigma 9$ twin boundary can produce a $\Sigma 3$ twin boundary, and a $\Sigma 27$ twin boundary can be formed. Higher-order twin boundaries between neighboring twins may appear at triple junctions. These twin boundaries contribute to the material’s hardening effect and lower the average free energy of dislocations.

The pinning effect of the strengthening phase on the grain boundary is determined by the interfacial energy of the grain boundary when it interacts with the strengthening phase, as described in Zener’s principle [33]. In nickel-based superalloys, the interfacial energy of high-angle grain boundaries is typically 0.69 J/m^2 . In contrast, coherent twin barriers have a much lower interface energy of only 0.03 J/m^2 . Consequently, the pinning effect of the strengthening phase on the twin boundary is relatively weaker. Figure 9 shows that the forgings contained additional subgrain boundaries and dislocation substructures. Twin boundaries are usually absent in recrystallized grains of smaller sizes but are more likely to appear in larger grains, suggesting that they form along with expanding recrystallized grains. The creation of twin boundaries is commonly observed at three-fork grain boundaries in forgings, as it reduces the system’s interface energy. The majority of the twin

boundaries in alloy forgings are primary three twin boundaries, with a few high-order $\Sigma 9$ twin boundaries and scarce high-order $\Sigma 27$ twin boundaries. The development of twin boundaries is also influenced by the degree of deformation, which promotes the nucleation of recrystallized grains. The most notable consequence of twin boundaries is the expansion of the grain boundary region, leading to enhanced alloy strength [34].

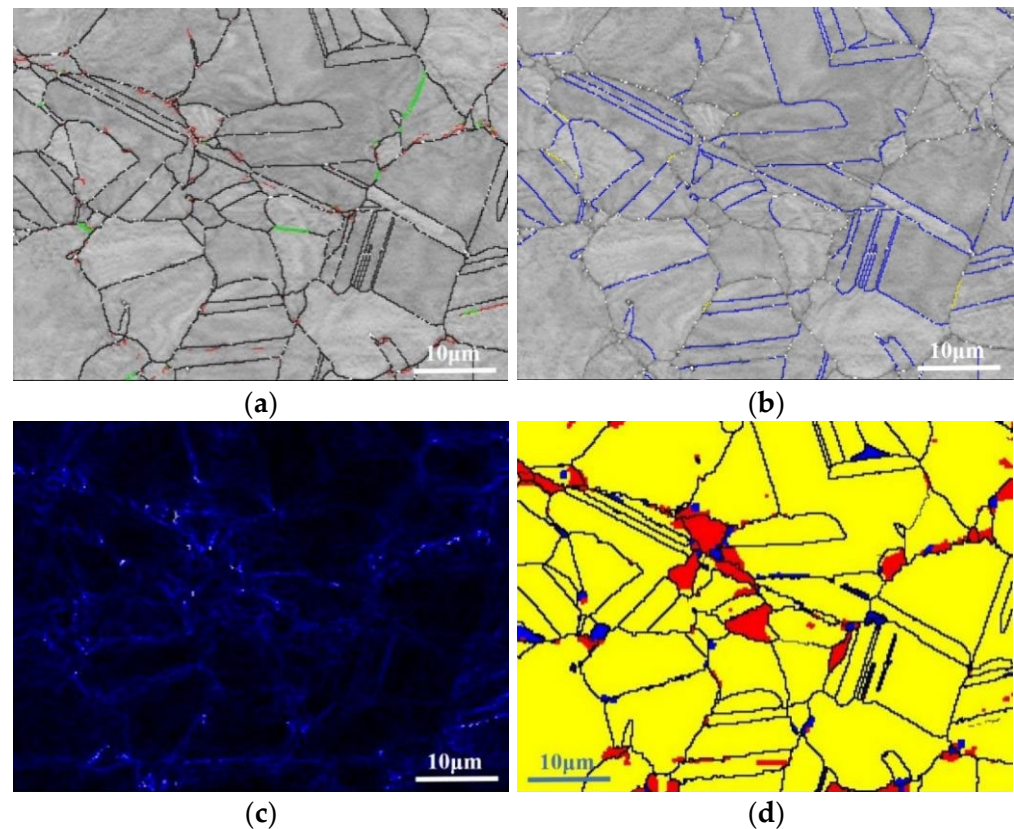


Figure 9. EBSD diagram of GH4738 alloy forgings with 80% deformation. (a) Angle diagram of orientation difference between grains ($>15^\circ$, $5\sim 15^\circ$, and $2\sim 5^\circ$ black line, green line, and red line are used in turn); (b) $\Sigma 3$, $\Sigma 9$ twin boundary (indicated by blue line and yellow line in turn); (c) dislocation density diagram between grains (increased from blue to white in turn); (d) distribution of recrystallized grains (indicated by blue, yellow, and red areas for complete recrystallization, substructure, and incomplete recrystallization in turn).

3.4. γ' Phase Evolution in Nickel-Based Superalloys

The alloy was enriched with approximately 4.5 wt% of Al and Ti elements, which combined to form the γ' phase. The γ' phase adopted a face-centered cubic ordered structure and could only exist in the matrix due to its compatibility with the matrix. The primary component of the γ' phase is $\text{Ni}_3(\text{Al}, \text{Ti})$, and the content and dissolution temperature of the γ' phase vary based on the Al and Ti content. In this study, the dissolution temperature of the Al + Ti element was approximately 1040°C [35,36]. The main method of strengthening the alloy was through the precipitation strengthening of the γ' phase. The performance of the alloy is heavily influenced by the quantity, distribution, and size of the γ' phase within it. In the research on strengthening GH4720Li alloy [37–39], two types of coupling cutting relationships were observed between the γ' phase and dislocations: strong coupling dislocation cutting and weak coupling cutting, depending on whether the particle size of the γ' phase was greater than or equal to 40 nm. It has been found that the optimum particle size for the γ' phase in the best precipitation strengthening state is 40 nm. Within this range, the critical shear stress value ranges from 70% to 100% of the peak value, indicating a significant strengthening effect. Even in the range of 30–100 nm, the particle size of the γ' phase still contributes to a notable strengthening impact. Although

there may be differences in composition and shape, the essential shear stress and particle size discussed above are also applicable to the γ' phase in the GH4738 alloy, as it differs from the γ' phase in the GH4720Li alloy primarily in terms of quantity.

The TEM image of the GH4738 alloy forgings in Figure 10 reveals a dislocation spacing of approximately 40 nm. The most effective strengthening occurred when the initial dislocation cut into the γ' phase, while the subsequent dislocation simply sheared off the γ' phase. This observation further confirms that 40 nm is the optimal particle size for the γ' phase, and this size significantly influences the precipitation strengthening of the alloy. Consequently, as the level of deformation increased, the size of the γ' phase particles and the spacing between them decreased, eventually converging toward 40 nm. This reduction in particle size and spacing enhanced the performance of the alloy.

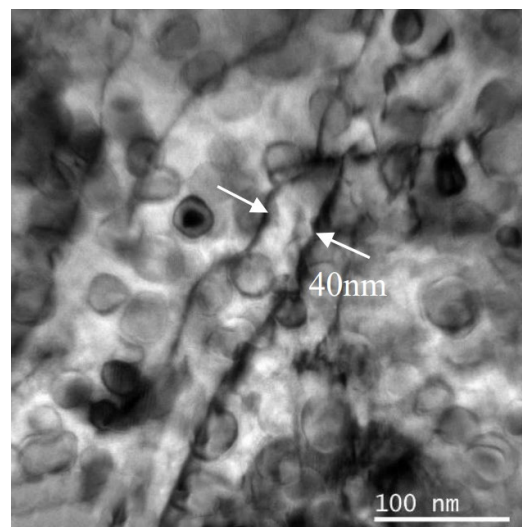


Figure 10. TEM image of GH4738 alloy forgings with an 80% deformation degree.

4. Conclusions

- (1) The grain size of nickel-based superalloys and the particle size of the “phase” steadily shrunk as the degree of deformation increased, and the hardness gradually rose. At 80% deformation, the hardness was 14.3% greater than it was at 62% distortion.
- (2) Chiseling and a limited amount of cutting were the major characteristics of high-temperature erosion at 750 °C, which was mostly dependent on the impact deformation mechanism. The sample with an 80% deformation degree had a lower high-temperature erosion rate, which was decreased by 10.3% when compared to the sample with a 62% deformation degree. Furthermore, the harder the alloy was, the faster it corroded at high temperatures.
- (3) The method of grain recrystallization used in Ni-based alloy forgings is known as discontinuous dynamic recrystallization, and it is characterized by a high dislocation density at the recrystallized grain boundaries. As a result, the sample’s microstructure frequently had numerous substructures and twin borders. This structure effectively refined the grains and increased the grain boundary area, which increased the alloy’s functionality even more.
- (4) As the degree of deformation increased during the hot working of the Ni-based alloy, the particle size and dislocation spacing of the phase decreased. According to studies, the ‘phase’s critical shear stress value is high, and its particle size ranges from 40 to 100 nm, which has a favorable strengthening impact on the alloy.

Author Contributions: Data curation, Z.C. and W.Z.; Writing—original draft, J.L.; Writing—review & editing, R.D.; Supervision, X.Z. All authors have read and agreed to the published version of the manuscript.

Funding: This research was funded by the Inner Mongolia Autonomous Region Science and Technology Plan Project, grant number 2021GG0266, and Inner Mongolia University of Technology 2022 Science and Technology Innovation Fund for Undergraduates, grant number 88.

Data Availability Statement: Data is contained within the article.

Conflicts of Interest: The authors declare no conflict of interest.

References

1. Qian, Y.-H.; Li, H.-K. *Superalloy*; Metallurgical Industry Press: Beijing, China, 2022; pp. 1–99.
2. Wang, H.-Y.; An, Y.-Q.; Li, C.-Y. Research Progress of Ni-based Superalloys. *Mater. Rep.* **2011**, *25*, 482–486.
3. Qu, J.-L.; Yi, C.-S.; Chen, J.-W. Research progress of precipitated phase in GH4720Li superalloy. *J. Mater. Eng.* **2020**, *48*, 73–83.
4. Du, J.; Zhao, G.; Deng, Q.; Lv, X.; Zhang, B. Development of Wrought Superalloy in China. *J. Aeronaut. Mater.* **2016**, *36*, 27–39.
5. Ma, J.; Li, W.; Zhang, X.; Kou, H.; Shao, J.; Geng, P.; Deng, Y.; Fang, D. Tensile properties and temperature-dependent yield strength prediction of GH4033 wrought superalloy. *Mater. Sci. Eng. A* **2016**, *676*, 165–172. [[CrossRef](#)]
6. Guo, J.-T. *Materials Science and Engineering for Superalloys*; Science Press: Beijing, China, 2010.
7. Shi, C.-X.; Zhong, Z.-Y. Development and innovation of superalloy in China. *Acta Metall. Sin.* **2010**, *46*, 1281–1288. [[CrossRef](#)]
8. Liu, Y.; Zhang, Y.-A.; Wang, W.; Li, D.-S.; Ma, J.-Y. Influence of rare earth Y on microstructure and high temperature oxidation behavior of Ni-Fe-Co-Cu alloy. *Chin. J. Rare Met.* **2020**, *44*, 9–15.
9. Velikanova, N.-P.; Protasova, N.-A.; Velikanov, P.-G.; Kiselev, A.S.; Salih, S.I.S. Influence of operating time on the strength reliability of the gas generator turbine disk of the aircraft drive for the GPA. *J. Phys. Conf. Ser.* **2021**, *1891*, 012044. [[CrossRef](#)]
10. Li, C.-M.; Tan, Y.-B.; Zhao, F. Modification of Flow Stress Curve and Processing Maps of Inconel 718 Superalloy. *Chin. J. Rare Met.* **2020**, *44*, 585–596.
11. Liu, W.-C.; Xiao, F.-R.; Yao, M.; Chen, Z.-L.; Jiang, Z.-Q.; Wang, S.-G. Relationship between the lattice constant of γ phase and the content of δ phase, γ'' and γ' phases in inconel 718. *Scr. Mater.* **1997**, *37*, 59–64. [[CrossRef](#)]
12. Yoo, B.; Im, H.-J.; Seol, J.-B.; Choi, P.-P. On the microstructural evolution and partitioning behavior of L12-structured γ' -based Co-Ti-W alloys upon Cr and Al alloying. *Intermetallics* **2019**, *104*, 97–102. [[CrossRef](#)]
13. Su, X.; Lv, X.-D. Thermal deformation behavior of as-cast and as-forged GH4738 alloy. *Heat Treat. Met.* **2021**, *46*, 46–52.
14. Li, H.-Y.; Dong, J.-X.; Li, L.-H. Evolution of microstructure and hot deformation behavior of GH4738 alloy during homogenization. *Trans. Mater. Heat Treat.* **2017**, *38*, 61–69.
15. Goodfellow, A.-J.; Galindo-Nava, E.-I.; Christofidou, K.-A.; Jones, N.G.; Boyer, C.D.; Martin, T.L.; Bagot, P.A.J.; Hardy, M.C.; Stone, H.J. The effect of phase chemistry on the extent of strengthening mechanisms in model Ni-Cr-Al-Ti-Mo based superalloys. *Acta Mater.* **2018**, *153*, 290–302. [[CrossRef](#)]
16. Dai, C.-W.; Ding, W.-F.; Xu, J.-H.; Fu, Y.-C.; Yu, T.-Y. Influence of Grain Wear on Material Removal Behavior during Grinding Nickel-based Superalloy with a Single Diamond Grain. *Int. J. Mach. Tools Manuf.* **2017**, *113*, 49–58. [[CrossRef](#)]
17. Li, W.; Yang, G.; Lei, T.; Yin, S.-B.; Wang, L. Hot Deformation Behavior of GH738 for A-USC Turbine Blades. *J. Iron Steel Res.* **2015**, *22*, 1043–1048.
18. Liu, H.; Cai, X.-Y. Effects of Hot Working Parameters on Dynamic Recrystallization Behaviors of GH738 Alloy. *J. Iron Steel Res.* **2014**, *26*, 46–50.
19. Jiang, H.; Li, Y.-J.; Liu, Q.-Y.; Dong, J.-X. Effect of Final Forging Temperature on Hot Deformation Behavior of GH4738 Superalloy. *Rare Met. Mater. Eng.* **2021**, *50*, 2552–2556.
20. Wang, L.-Y.; Wang, J.-G.; Liu, D.; Wang, H.-P.; Xu, W.-S.; Zhao, X.-D.; Tong, J.; Qin, W.-D. Characterization and verification on hot working process windows for GH4738 alloy. *Forg. Stamp. Technol.* **2021**, *46*, 207–215.
21. Wang, W.-W.; Yi, Y.-P.; Li, P.-C.; Huang, S.-Q. Simulation on Forging Process for Superalloy Waspaloy Turbine Disc Using Composite Sheathed Technology. *Hot Work. Technol.* **2011**, *40*, 22–25.
22. Kvackaj, T.; Zrnik, J.; Vrchovinsky, V. Influence of plastic deformation on creep behaviour of NiMoCr alloy. *High Temp. Mater. Process.* **2003**, *22*, 57–62. [[CrossRef](#)]
23. Wang, H.-P.; Liu, D.; Shi, Y.-Z.; Wang, J.; Yang, Y.; Wang, L.; Qin, W. Matrix-Diffusion-Controlled Coarsening of the γ' Phase in Waspaloy. *Met. Mater. Int.* **2019**, *25*, 1410–1419. [[CrossRef](#)]
24. Yao, Z.-H.; Dong, J.-X.; Zhang, M.-C.; Hong, C.-M. Influence of solution and stabilization heat treatment on carbide and gamma prime for super alloy GH738. *Trans. Mater. Heat Treat.* **2013**, *34*, 43–49.
25. Jackson, M.P.; Reed, R.C. Heat treatment of UDIMET 720Li: The effect of microstructure on properties. *Mater. Sci. Eng. A* **1999**, *259*, 85–97. [[CrossRef](#)]
26. Decker, R. The evolution of wrought age-hardenable superalloys. *JOM* **2006**, *58*, 32–36. [[CrossRef](#)]
27. Azarbarmas, M.; Aghaie-Khafri, M.; Cabrera, J.M.; Calvo, J. Dynamic recrystallization mechanisms and twinning evolution during hot deformation of Inconel 718. *Mater. Sci. Eng. A* **2016**, *678*, 137–152. [[CrossRef](#)]
28. Drapier, J.; Coutouradis, D.; Habraken, L. Measurements of stacking-fault energies in CoNi and CoNi-Cr alloys. *Acta Metall.* **1967**, *15*, 673–675. [[CrossRef](#)]
29. Wan, Z.-P. Study on High Temperature Deformation Behavior and Microstructure and Properties Control of GH4720LI Nickel-Based Alloy. Ph.D. Thesis, Harbin Institute of Technology, Harbin, China, 2019.

30. Xiang, S.; Ju, Q.; Liu, G.-Q. Dynamic recrystallization mechanism of 15Cr-25Ni-Fe base superalloy. *J. Jiangsu Univ.* **2010**, *31*, 665–669.
31. Shi, C.-Y.; Zhang, M.-C.; Guo, J. Recrystallization Mechanism of Typical Ni-based Superalloys. *Rare Met. Mater. Eng.* **2023**, *52*, 63–73.
32. Chen, X.-F.; Yao, Z.-H.; Dong, J.-X.; Shen, H.-W.; Wang, Y. The effect of stress on primary MC carbides degeneration of Waspaloy during long term thermal exposure. *J. Alloys Compd.* **2018**, *735*, 928–937. [[CrossRef](#)]
33. Zener, C.; Hollomon, J.H. Effect of Strain Rate Upon Plastic Flow of Steel. *J. Appl. Phys.* **1944**, *15*, 22–32. [[CrossRef](#)]
34. Chen, Z.-S. Effect of Hot Working Process on Microstructure and Properties of GH4738 Superalloy. Master's Thesis, Inner Mongolia University of Technology, Hohhot, China, 2021.
35. Chen, Z.-Q.; Tai, Q.-A.; Zhao, X.-D.; Wang, J.-Y.; Li, C.-Y. Precipitation and dissolution on carbide for superalloy GH738. *J. Iron Steel Res.* **2013**, *25*, 37–45.
36. Liu, X.-B.; Wang, T.; Chen, S.; Wei, K.; Fu, S.-H.; Li, Z.; Wan, Z.-P. Effect of Al and Ti elements on γ' phase dissolution law of GH4738 alloy during heat treatment. *Hot Work. Technol.* **2022**, *51*, 93–96.
37. Chen, Z.S.; Dong, R.F.; Li, J.N.; Deng, X.T.; Zhang, W.; Ren, X.L. Reasons for the stable existence of gamma' phase and strengthening mechanism of GH4720Li nickel-based superalloy. *Mater. Res. Express* **2021**, *8*, 056508.
38. Li, J.-N. Effect of Hot Working Technology on Microstructure and Properties of GH4720Li Superalloy and Research on Its Mechanism. Master's Thesis, Inner Mongolia University of Technology, Hohhot, China, 2020.
39. Zhang, W.; Li, J.-N.; Dong, R.-F.; Chen, Z.-S.; Li, J.; Zhou, X.; Wang, Q.-Z.; Qu, J.-L. Effect of heat treatment process parameters on the microstructure and properties of GH4720Li superalloy. *Mater. Res. Express* **2023**, *10*, 016514.

Disclaimer/Publisher's Note: The statements, opinions and data contained in all publications are solely those of the individual author(s) and contributor(s) and not of MDPI and/or the editor(s). MDPI and/or the editor(s) disclaim responsibility for any injury to people or property resulting from any ideas, methods, instructions or products referred to in the content.